

Pair-sphere trajectories in finite-Reynolds-number shear flow

PANDURANG M. KULKARNI AND JEFFREY F. MORRIS

Benjamin Levich Institute and Department of Chemical Engineering, The City College
of New York, New York, NY 10031, USA

(Received 24 March 2007 and in revised form 15 October 2007)

The pair trajectories of neutrally buoyant rigid spheres immersed in finite-inertia simple-shear flow are described. The trajectories are obtained using the lattice-Boltzmann method to solve the fluid motion, with Newtonian dynamics describing the sphere motions. The inertia is characterized by the shear-flow Reynolds number $Re = \rho \dot{\gamma} a^2 / \mu$, where μ and ρ are the viscosity and density of the fluid respectively, $\dot{\gamma}$ is the shear rate and a is the radius of the larger of the pair of spheres in the case of unequal sizes; the majority of results presented are for pairs of equal radii. Reynolds numbers of $0 \leq Re \leq 1$ are considered with a focus on inertia at $Re = O(0.1)$. At finite inertia, the topology of the pair trajectories is altered from that predicted at $Re = 0$, as closed trajectories found in Stokes flow vanish and two new forms of trajectories are observed. These include spiralling and reversing trajectories in addition to largely undisturbed open trajectories. For $Re = O(0.1)$, the limits of the various regions in pair space yielding open, reversing and spiralling trajectories are roughly defined.

1. Introduction

Suspension mechanics is based in large part upon understanding the hydrodynamic interactions between particles suspended in viscous fluid. For simplicity the particles considered are usually spherical. Hence, the relative motion of spheres is central to the study of suspension mechanics. Batchelor & Green (1972) studied this problem for a pair of neutrally buoyant spheres moving freely, i.e. experiencing zero force and zero torque, in a linear Stokes flow. This work followed a body of studies which considered the specific case of hydrodynamic interaction of two spheres immersed in an ambient shear field (see for example Wakiya, Darabaner & Mason 1967; Lin, Lee & Sather 1970*a*; Brenner & O'Neill 1972). The results of this work, directly and through formal extension to a system of hydrodynamic functions computed to high accuracy (Jeffrey & Onishi 1984; Kim & Mifflin 1985; Jeffrey 1992), provide the basis for not only analytical studies (Batchelor 1977; Brady & Morris 1997; Zarraga & Leighton 2001), but also for simulation tools such as Stokesian Dynamics (Brady & Bossis 1988) and related approaches (Ladd 1988) which address many particles at a wide range of solid fraction. Darabaner & Mason (1967) experimentally addressed the hydrodynamic interaction of two spheres of equal as well as unequal size suspended in a circular Couette flow at the low-particle Reynolds number of $O(10^{-6})$. Darabaner & Mason showed that, depending on the separation between the two spheres, they will either orbit around each other (permanent collision) or separate, a result in agreement with the analysis of Batchelor & Green (1972).

Viscous suspensions have thus been well studied and there is now a body of understanding of their behaviour, including the transport properties of rheology and self-diffusion, as well as such bulk flow phenomena as shear-induced migration. As a model two-phase material, the Stokes-flow suspension has played a valuable role in the development of the study of mixture flow. However, progress in understanding mixture flow at finite inertia has been slow (Koch & Hill 2001). New computational techniques have recently made examination of motions of interacting particles at finite Reynolds number feasible. Because of the computational costs involved, the conventional computational fluid dynamics (CFD) methods such as finite element applied to the particle-laden flow (Hu, Joseph & Crochet 1992; Hu 1996; Hu, Patankar & Zhu 2001) have to date largely examined two-dimensional particle-laden flows with finite inertia (Feng, Hu & Joseph 1994; Huang & Joseph 2000), with sedimentation the most commonly considered flow. Three-dimensional problems studied include the settling ellipsoid in a tube with boundary interactions accounted for (Swaminathan, Mukundakrishnan & Hu 2006). There is associated with the finite-element method (FEM) the requirement of remeshing the fluid as the structure evolves, and the extremely small surface separations to which particles are driven in shear flow magnify this problem. We choose to work with the lattice-Boltzmann method (LBM) as developed for particulate flows (Ladd 1994*a, b*; Aidun, Lu & Ding 1998; Ladd & Verberg 2001). In this method, the particles move on a fixed mesh, which simplifies the problem relative to FEM, while allowing simulation of finite inertia fluid motion and thus providing capability not available in Stokesian Dynamics. The spatial locality of the lattice-Boltzmann equation, and the fixed grid provide ease of parallelization. A potential disadvantage of the LBM is that because of its formulation it allows finite compressibility of the fluid, as discussed in §2.3, and care must be taken when simulating incompressible motions to ensure that the influence of compressibility is small. We present quantitatively the effect of finite compressibility on our results in §4.1.

The problem addressed here is that of determining the relative motion of pairs of spheres in finite-Reynolds-number shear flow. Only the case of neutrally buoyant particles will be considered. The Reynolds number characterizing the fluid inertia in shear is given by $\rho\dot{\gamma}a^2/\mu$, where a is the particle size (taken as the radius for a sphere), μ and ρ are the viscosity and density of the fluid, respectively, and $\dot{\gamma}$ is the shear rate. The particles, being of equal density to the fluid, have similar inertia to the fluid. However, we emphasize that Re is related to fluid inertia to distinguish it from the Stokes number, which may be written $St = (\rho_p/\rho)Re$, using ρ_p to denote the density of the particle; St characterizes particle inertia. Only recently has there appeared work addressing the influence of inertia on the relative motion of particle pairs in shear flow, and all of the work of which we are aware has considered cases different from the present study. This recent work is numerical and we know of no experiments addressing the issue, although the influence of finite-inertial hydrodynamic interactions has been suggested to play a role in experimentally observed formation of chain-like structures in dilute pressure-driven suspension flow in a pipe by Matas *et al.* (2004), a phenomenon replicated in square duct flow simulations (Chun & Ladd 2006). The numerical work noted includes the case[†] of $St > 0$ and

[†] Subramanian & Brady (2006) used $St^* = 2St/9$ and the same Re as presented in this work, but we prefer the definition of Stokes number given here as it indicates excess particle inertia if St exceeds Re , whereas the equivalent physically significant condition is found when $St^* > 2Re/9$.

$Re \equiv 0$ studied by Subramanian & Brady (2006) while $St > Re > 0$ was considered by Kromkamp *et al.* (2005). Subramanian & Brady used well-known hydrodynamic interaction functions to determine the hydrodynamic force and torque on particles with finite values of St , corresponding perhaps to solid particles in gas, and observed a rich set of new features including limit cycles in the pair trajectory space relative to the zero- Re -zero- St condition. The Kromkamp *et al.* study considered two-dimensional circular cylinders at $0 < Re \leq 0.51$, with $\rho_p/\rho = 3$ and 10 yielding $St = 3Re$ or $10Re$. The combined influence of fluid inertia and excess particle inertia (i.e. $St > Re$) results in behaviour which differs from the neutrally buoyant case examined in this study. Because the conditions of both the Subramanian & Brady and the Kromkamp *et al.* studies involved heavy particles, gravity was neglected in their work. Here, we study the case of neutrally buoyant particles because it seems the first natural case to examine in order to isolate the role of inertia in shear-induced hydrodynamic interactions, and furthermore because the conditions are experimentally realizable in normal gravity.

The fluid flow around a single sphere in simple-shear flow at finite inertia has been studied analytically (Lin, Peery & Schowalter 1970*b*), experimentally (Poe & Acrivos 1975) and numerically (Nirschl, Dwyer & Denk 1995 by finite volume; Mikulencak & Morris 2004 by finite element). An important aspect of the flow characteristics of this simplest system was missed in these prior studies, as shown by the recent analysis of Subramanian & Koch (2006*a, b*). These authors showed that the streamline topology at finite Re changes qualitatively from that at $Re = 0$. In particular, the fluid elements close to the freely rotating sphere spiral outward rather than forming a closed streamline region. This leads to the prediction that the suspended particles significantly enhance heat and mass transfer, by introducing a convective mechanism rather than diffusion through the closed-streamline zone. We apply the LBM to gain further insight into the finite- Re streamline pattern around a single sphere in support of the primary goal of understanding pair-sphere trajectories in shearing flows. Pair trajectories at small Re are found to be similar in their structure, even for equal-sized spheres, to the streamlines around the single sphere.

In §2, we define the problem and present a brief outline of the methods used in our study. We then present our simulation results, examining the streamlines around a single sphere (§3) and pair trajectories of spheres (§4) in simple-shear flow at finite inertia.

2. Problem statement and solution method

2.1. Governing equations

Our interest is in the motion of neutrally buoyant solid spherical particles suspended in a Newtonian fluid subjected to simple shear flow with finite fluid inertia. The governing equations in non-dimensional form for the fluid phase are

$$\nabla \cdot \mathbf{u} = 0, \quad (2.1a)$$

$$Re \left(\frac{\partial \mathbf{u}}{\partial t} + \mathbf{u} \cdot \nabla \mathbf{u} \right) = -\nabla p + \nabla^2 \mathbf{u}, \quad (2.1b)$$

where length has been made dimensionless with the radius of the sphere a , time by the inverse of the shear rate $\dot{\gamma}^{-1}$, fluid velocity by $\dot{\gamma}a$, and the pressure by $\mu\dot{\gamma}$. The shear-flow Reynolds number is defined as $Re = \rho\dot{\gamma}a^2/\mu$, where μ and ρ are, respectively, the viscosity and density of the fluid. Particle translations (\mathbf{U}_i) and rotations ($\boldsymbol{\Omega}_i$) are

governed by Newtonian dynamics,

$$m_i \frac{\partial \mathbf{U}_i}{\partial t} = \mathbf{F}_i, \quad (2.2a)$$

$$I_i \frac{\partial \boldsymbol{\Omega}_i}{\partial t} = \mathbf{T}_i, \quad (2.2b)$$

where the net force \mathbf{F}_i and net torque \mathbf{T}_i act on the particle i , which has mass and moment of inertia m_i and I_i , respectively. We shall focus on the relative motion of a pair of neutrally buoyant spherical particles, with certain results presented for a single sphere to facilitate understanding of the pair problem.

2.2. Limiting behaviour: Stokes solutions

Before proceeding to the solution method, we recall the well-known limiting behaviour obtained analytically at $Re=0$ for the isolated sphere and a pair of equally sized spheres. At $Re=0$, the flow field around a sphere suspended in simple-shear flow may be obtained analytically via superposition of vector harmonic functions (Leal 1992). The velocity field in the fluid around the sphere is given by Mikulencak & Morris (2004) as

$$u_x = \frac{1}{2}y(1 - r^{-5}) + \frac{1}{2}y(1 - r^{-3}) - \frac{5}{2}x^2y(r^{-5} - r^{-7}) - \frac{\Omega y}{r^3}, \quad (2.3a)$$

$$u_y = \frac{1}{2}x(1 - r^{-5}) - \frac{1}{2}x(1 - r^{-3}) - \frac{5}{2}y^2x(r^{-5} - r^{-7}) + \frac{\Omega x}{r^3}, \quad (2.3b)$$

$$u_z = -\frac{5}{2}xyz(r^{-5} - r^{-7}). \quad (2.3c)$$

If the sphere rotates freely (zero torque), it has steady angular velocity, made dimensionless with $\dot{\gamma}$, of $\Omega = 1/2$, matching the vorticity of the undisturbed flow. The inertialess streamline configuration around the freely rotating sphere is shown in figure 1(a). The flow is characterized by a region of closed streamlines which extends infinitely in both the flow and vorticity directions. Outside this closed streamline region, open streamlines begin from upstream infinity, and proceed past the particle to downstream infinity, e.g. beginning from $(x \rightarrow -\infty, y > 0)$ and proceeding to $(x \rightarrow \infty, y > 0)$. The streamline form is mirrored through the plane $y=0$. All streamlines, whether open or closed, also have fore–aft symmetry about the plane $x=0$, owing to the linearity and reversibility of the Stokes equations.

The relative trajectories of a pair of particles in Stokes flow have a number of similarities to the streamlines around an isolated sphere. Two spherical particles suspended freely in simple-shear flow at $Re=0$ follow one of two kinds of pair trajectories. These are illustrated for equally sized spheres in figure 1(b). One type are the ‘open’ trajectories in which one particle starts far upstream with an offset in the gradient direction, approaches and passes over the other particle and returns to the same offset far downstream. The second type are ‘closed’ trajectories in which the particles are captured in permanent orbits around each other. The region occupied by the closed trajectories has infinite volume (Batchelor & Green 1972). Nonetheless, the set of closed trajectories is compressed to a very narrow band where the pair separation is only slightly greater than two radii on closest approach, as seen in figure 1(b). A closed surface, symmetric about the planes $x=0$ and $y=0$, separates these two regions in trajectory space; the same symmetries about these planes hold for all pair trajectories in Stokes flow. The open and closed trajectories are found for arbitrary size ratio of the two spheres, i.e. a and $b \neq a$, and in the limit of $b/a \ll 1$ the smaller sphere should asymptotically follow the fluid motion around an isolated sphere. There is thus a continuous variation from the streamline about a single sphere to the trajectory of a pair of equal sized spheres.

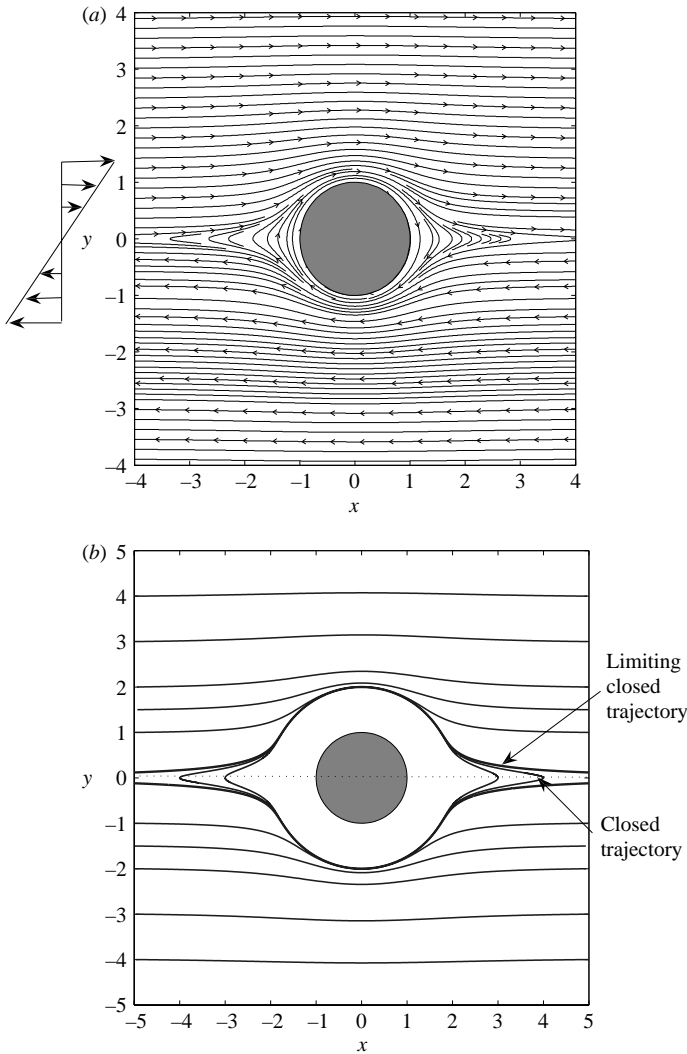


FIGURE 1. (a) Streamline configuration around a freely rotating sphere in simple-shear flow at $Re=0$. (b) Pair trajectories of two force-free spheres in simple-shear flow at $Re=0$ obtained from the analytical solution of Batchelor & Green (1972): the curves describe the motion of a second sphere relative to the origin instantaneously fixed at the centre of the first (as indicated by the grey circle at the origin). For both (a) and (b) shear flow of form $u_x = \dot{\gamma}y$ is as indicated in (a).

2.3. Lattice-Boltzmann method

We use the approach of Ladd (Ladd 1994a, b; Aidun *et al.* 1998; Ladd & Verberg 2001) for the LBM to model the fluid motion in this work. The LBM when applied to a suspension combines Newtonian mechanics for the solid particles with a discretized Boltzmann model for the fluid. The fluid phase is discretized in space and time and is taken to be made of fictitious particles (or ‘LB particles’) which are constrained to move on a regular lattice. The state of the system is characterized by the one-particle velocity distribution function $n_i(\mathbf{r}, t)$, which describes the mass density of the LB particles moving with discrete velocity \mathbf{c}_i at a lattice node \mathbf{r} at time t . We have used

the three-dimensional, 19-velocity, or D3Q19, velocity model in which a particle can either rest or move to the nearest (directly along a lattice direction, e.g. [100]) or diagonally next nearest (e.g. [110]) neighbouring node of a cubic lattice (Ladd & Verberg 2001). The mass density ρ , momentum density $\mathbf{j} = \rho \mathbf{u}$ and the momentum flux Π are defined by moments of the velocity distribution function

$$\rho = \sum_i n_i, \quad \mathbf{j} = \sum_i n_i \mathbf{c}_i, \quad \Pi = \sum_i n_i \mathbf{c}_i \mathbf{c}_i. \quad (2.4)$$

The lattice-Boltzmann equation for the evolution of $n_i(\mathbf{r}, t)$ is written as (Frisch *et al.* 1987; Higuera, Succi & Benzi 1989; Ladd 1994a)

$$n_i(\mathbf{r} + \mathbf{c}_i \Delta t, t + \Delta t) = n_i(\mathbf{r}, t) + \sum_j \Omega_{ij} n_j^{neq}, \quad (2.5)$$

where Δt is the time step and the collision operator Ω_{ij} describes the change in n_i due to collisions. The non-equilibrium distribution function is defined as $n_i^{neq} = n_i - n_i^{eq}$. The general form of equilibrium distribution is chosen to recover the Navier–Stokes equations for low Mach number flows ($Ma = u/c_s \ll 1$, where $c_s = \sqrt{1/3}$ is the speed of sound in lattice units) and can be written to $O(u^2)$ as (Ladd & Verberg 2001)

$$n_i^{eq} = a^{c_i} \left[\rho + \frac{\mathbf{j} \cdot \mathbf{c}_i}{c_s^2} + \frac{\rho \mathbf{u} \mathbf{u} : (\mathbf{c}_i \mathbf{c}_i - c_s^2 \mathbf{I})}{2c_s^4} \right], \quad (2.6)$$

where \mathbf{I} is the identity tensor and a^{c_i} are the coefficients of three speeds 0, 1 and $\sqrt{2}$ associated, respectively, with LB particles remaining at the same node, moving to a nearest neighbour, or moving to a next-nearest neighbour. At equilibrium the density of lattice-Boltzmann particles moving in the [100] direction is twice that for the [110] direction and hence the coefficients, obtained from conservation constraints, are given by $a^0 = \frac{1}{3}$, $a^1 = \frac{1}{18}$, and $a^{\sqrt{2}} = \frac{1}{36}$. The post-collision distribution $n_i^*(\mathbf{r}, t)$ is written as a series of moments,

$$n_i^* = a^{c_i} \left[\rho + \frac{\mathbf{j} \cdot \mathbf{c}_i}{c_s^2} + \frac{(\rho \mathbf{u} \mathbf{u} + \Pi^{neq,*}) : (\mathbf{c}_i \mathbf{c}_i - c_s^2 \mathbf{I})}{2c_s^4} \right]. \quad (2.7)$$

In the collision process mass and momentum remain conserved but the non-equilibrium momentum flux changes according to

$$\Pi^{neq,*} = (1 + \lambda) \bar{\Pi}^{neq} + \frac{1}{3} (1 + \lambda_v) (\Pi^{neq} : \mathbf{I}) \mathbf{I}, \quad (2.8)$$

where λ and λ_v are eigenvalues of the collision operator and are related to the shear and bulk viscosities. After the collision, the population densities are streamed to the neighbouring node along velocity link \mathbf{c}_i .

In the LBM, solid particles are discretized in space and are defined by a surface that cuts some links between lattice nodes. Following Aidun *et al.* (1998), the fluid is removed from the interior of the particle. To implement solid–fluid boundary conditions the ‘link–bounce-back’ rule, in which the boundary nodes are located midway between the solid and the fluid nodes, is applied. The population densities of the fluid nodes just outside the solid surface are modified such that the fluid velocity is matched to the local solid velocity. We consider a set of fluid nodes at position defined by \mathbf{r} and for each node all the velocities \mathbf{c}_i such that $\mathbf{r} + \mathbf{c}_i \Delta t$ lies inside the particle surface. If $\mathbf{r}_b = \mathbf{r} + \frac{1}{2} \mathbf{c}_i \Delta t$ is a point inside the particle moving with translation \mathbf{U} and angular speed $\boldsymbol{\Omega}$, then its velocity is

$$\mathbf{u}_b = \mathbf{U} + \boldsymbol{\Omega} \times (\mathbf{r}_b - \mathbf{R}), \quad (2.9)$$

where \mathbf{R} is the centre of mass of the particle. The population density is updated by

$$n_{-i}(\mathbf{r}, t + \Delta t) = n_i^*(\mathbf{r}, t) - \frac{2a^{c_i} \rho_0 \mathbf{u}_b \cdot \mathbf{c}_i}{c_s^2}, \quad (2.10)$$

where $-i$ denotes the velocity $\mathbf{c}_{-i} = -\mathbf{c}_i$. In this update momentum is exchanged between the solid and the fluid particle, but the combined momentum is conserved. The force exerted at the boundary node is given by

$$\mathbf{f}_b(\mathbf{r}_b, t + \frac{1}{2}\Delta t) = \frac{\Delta x^3}{\Delta t} \left[2n_i^* - \frac{2a^{c_i} \rho_0 \mathbf{u}_b \cdot \mathbf{c}_i}{c_s^2} \right] \mathbf{c}_i, \quad (2.11)$$

where Δx is the lattice spacing. By summing over all the boundary nodes \mathbf{r}_b , we obtain the total force and torque acting on the particle as

$$\mathbf{F} = \sum_{\mathbf{r}_b} \mathbf{f}_b, \quad \text{and} \quad \mathbf{T} = \sum_{\mathbf{r}_b} \mathbf{f}_b \times \mathbf{r}_b. \quad (2.12)$$

The particle positions and velocities are then updated.

Since a suspended particle is represented discretely, it samples different numbers of nodes as it moves, and hence there is an effective hydrodynamic radius r_h which is greater than the prescribed radius a . This r_h depends only on a and fluid viscosity (Ladd & Verberg 2001). As the particle becomes large, the difference between r_h and a grows small; r_h is calibrated by calculating the drag coefficient of a sphere in the Stokes flow regime (Ladd 1994*b*).

An important part of the hydrodynamic interaction of two spheres involves near-field lubrication stresses, particularly due to squeeze flow associated with motion of a pair approaching contact along the line of centres. Though LBM can capture hydrodynamics down to one lattice spacing, the grid resolution may become insufficient to resolve the flow in the gap. To overcome this problem, Nguyen & Ladd (2002) proposed the following normal force be added between the two spheres:

$$\mathbf{F}_{lub} = -\frac{6\pi\mu(ab)^2}{(a+b)^2} \hat{\mathbf{r}} \hat{\mathbf{r}} \cdot \mathbf{U}_{21} \left(\frac{1}{h} - \frac{1}{h_c} \right), \quad (2.13)$$

where a and b are the radii of the spheres, $\mathbf{r} = \mathbf{x}_2 - \mathbf{x}_1$ for particles centred at \mathbf{x}_1 and \mathbf{x}_2 with $\hat{\mathbf{r}} = \mathbf{r}/|\mathbf{r}|$, and $\mathbf{U}_{21} = \mathbf{U}_2 - \mathbf{U}_1$ is the relative velocity of the pair. The gap $h = |\mathbf{r}| - 2a$ (or $h = |\mathbf{r}| - a - b$ for unequal sizes) is between the points of closest approach of the surfaces with h_c a cutoff for the added lubrication force: for gaps larger than h_c , $\mathbf{F}_{lub} = 0$, and this cutoff h_c is set empirically as $2/3$ of the lattice spacing.

3. Single particle at finite Re

It has recently been shown that for a single sphere rotating freely in simple-shear flow, the closed streamline structure present at $Re = 0$ is destroyed by weak inertia (Subramanian & Koch 2006*a, b*). The fluid elements close to the sphere spiral around it before departing the vicinity of the sphere to proceed ‘downstream.’ As shown below, the exit from the vicinity of the particle can be in either of the two possible directions associated with the shear flow $u_x = y$ depending upon which streamline is considered, i.e. there is an interlacing of streamlines which depart in the two directions. The rate of spiralling depends upon the value of Re . Accompanying the spiralling motion, mass conservation demands a net flux of the fluid along the vorticity direction toward the sphere, and these streamlines also spiral outward. Fluid outside the envelope of the spiralling region may either pass the body on an open streamline, or reverse its path;

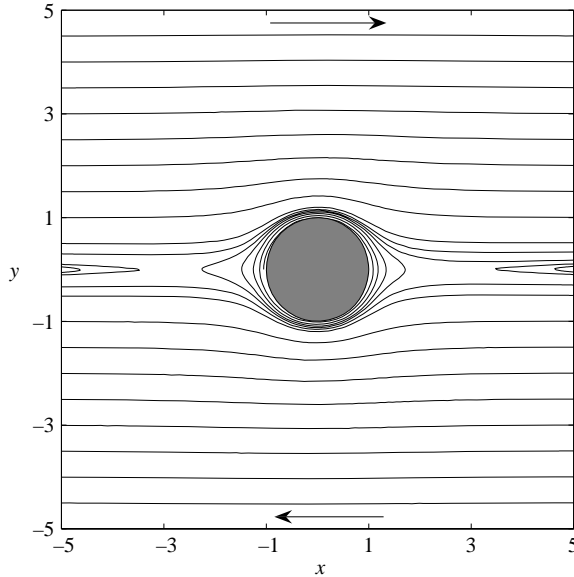


FIGURE 2. Computed streamline configuration in the plane of shear around a freely rotating sphere in simple-shear flow at $Re = 0.1$.

the reversal zone, discussed in detail by Mikulencak & Morris (2004), is associated with small gradient direction offsets sufficiently far upstream of the body to be outside the spiralling streamline region. A similar picture prevails as one considers planes of constant z , i.e. progressing in the vorticity direction, although the cross-section in the local x - y plane of the spiralling trajectories diminishes in size with increasing z . Streamlines in the plane of shear ($z = 0$), with the flow computed by the LBM, around a freely rotating sphere at $Re = 0.1$ are shown in figure 2. Note that the streamlines near the body make circuits and then depart from the particle toward infinity, and that reversing streamlines are evident at the left and right of the figure.

As Re increases, the reversing region approaches the particle (Mikulencak & Morris 2004) and the spiralling region collapses. This behaviour of the streamline pattern is quite similar to the case of a cylinder in two-dimensional flow (Robertson & Acrivos 1970; Kossack & Acrivos 1974). However, in the two-dimensional flow, the constraints of symmetry and incompressibility ensure that the streamlines close to the cylinder are closed. We plot in figure 3 fluid streamlines starting from the same point, specifically $(x, y, z) = (-1.3, 0, 0)$, for $Re = 0.05, 0.5$ and 5 . At lower Re , a fluid element makes more circuits around the sphere before it moves away permanently, and the direction of departure may be either left or right depending on the precise location of the initial point and the level of inertia. Figure 4 shows that the out-of-plane reversing (1) and open (2) fluid paths always tend to have a net displacement away from the shear plane while a spiralling streamline (3) comes closer to the shear plane before it departs the vicinity of the particle. Note that when they approach closely to the sphere, the spiralling paths have a portion on each circuit moving away from the sphere, but the net motion on a circuit is toward the body until the final circuit. On this final circuit, the net z -directed motion is slightly away from the body, and this will be echoed in the particle pair trajectories. The three-dimensional picture of the various forms of streamlines is illustrated in figure 5 for $Re = 0.5$, where single open, reversing, in- and out-of-plane spiralling fluid paths are plotted.

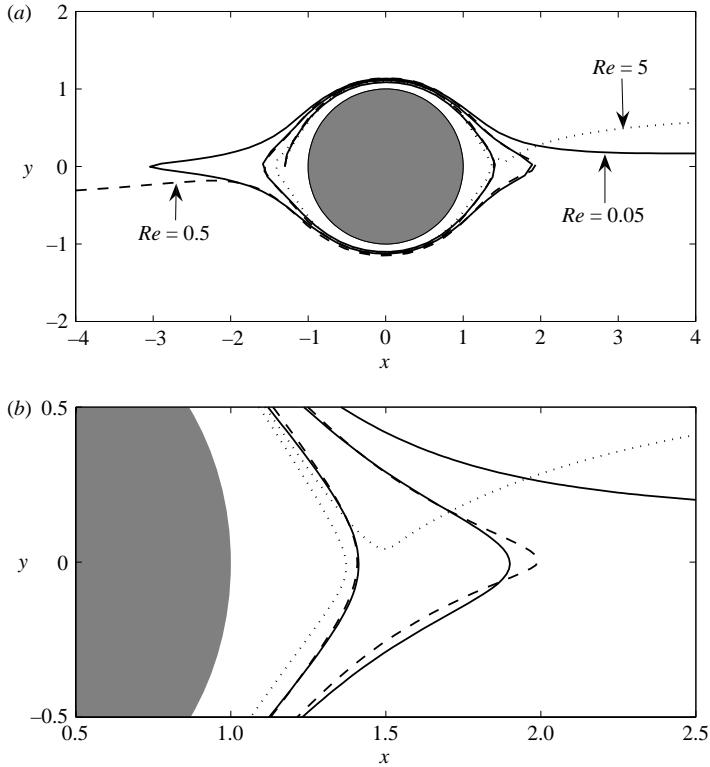


FIGURE 3. (a) Streamlines starting from $(-1.3, 0, 0)$ for $Re = 0.05, 0.5$ and 5 in simple-shear flow around a freely rotating sphere. (b) Expanded view of the region $(0.5 \leq x \leq 2.5, -0.5 \leq y \leq 0.5)$.

4. Pair trajectories at finite Re

Here, the aim is to determine the finite- Re trajectories of two spheres freely suspended in simple-shear flow. In most of the simulations discussed, two neutrally buoyant spheres of equal radius a are placed symmetrically in a computation box of size $L \times H \times W$, as illustrated in the sketch of figure 6; in some instances, we consider unequal spheres of a and $b < a$. The shear flow is set by moving the top and bottom walls in opposite directions at equal speed. Periodic boundary conditions are applied in the flow and vorticity directions; as in the prior discussion, x, y and z denote the flow, gradient and vorticity directions of the undisturbed flow, respectively. The spheres, initially separated by some displacement, are first allowed only to rotate until they achieve a steady flow field and are then released. The Mach number is defined by $Ma = \dot{\gamma}H/(2c_s)$, where $\dot{\gamma}H/2$ is the wall velocity. We maintain $Ma < 0.1$ in order to minimize compressibility effects. The constraint may be written $Ma = (\mu Re / \rho c_s a) \times (H/a) < 0.1$, which means that one has to decrease the viscosity of the fluid in order to increase Re for fixed a/H .

The primary interest here is in the role of fluid mechanical inertia upon the pair relative trajectory, and hence the shear Reynolds number Re is the key parameter determining the structure of the trajectory space. However, because we compute the motion in a periodic and wall-bounded domain, the nature of trajectories depends to some degree upon the domain size. Issues include the fact that walls suppress the rotation of a single particle in the shear flow by creating stronger flow reversal

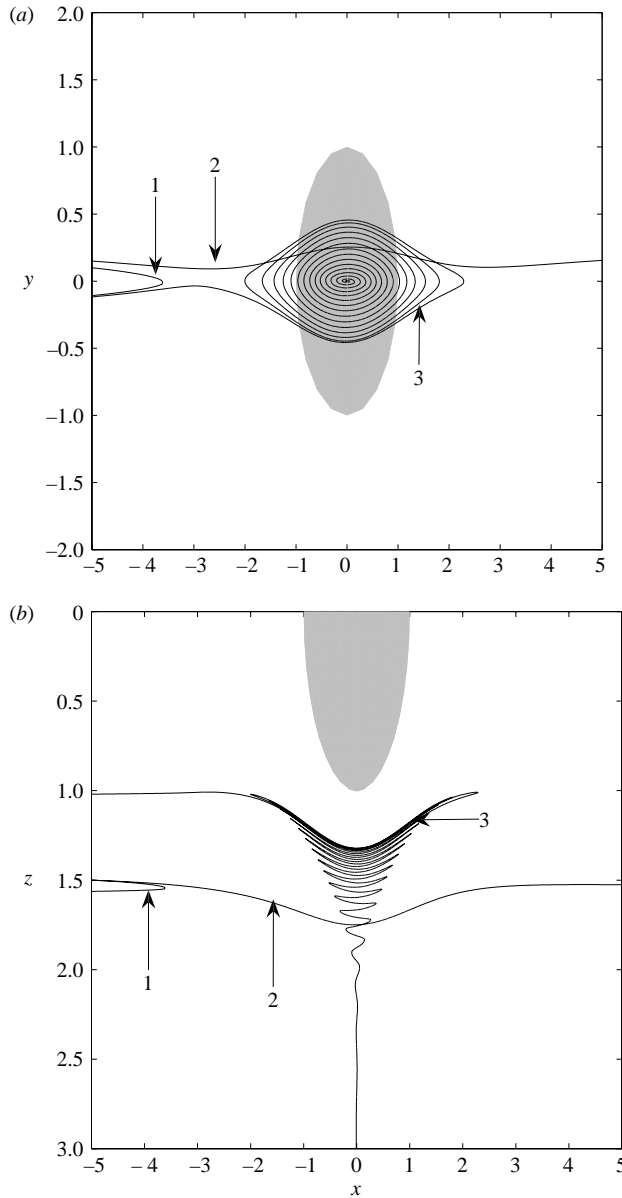


FIGURE 4. Off-plane fluid streamlines for $Re=0.1$ around a freely rotating sphere in simple-shear flow: (a) xy -projection; (b) xz -projection. (1) Reversing streamline originating from $(-5, 0.1, 1.5)$. (2) Open streamline originating from $(-5, 0.15, 1.5)$. (3) Spiralling streamline originating from $(-0.01, 0, 3.0)$. The spherical particle is shown as a shaded ellipse because of the stretched y or z coordinate.

regions (Ding & Aidun 2000); also, the particles interact with their periodic images, which gives rise to a dependence of trajectories on the size of the domain in flow and vorticity directions. Even in the absence of inertia, the presence of nearby walls will cause flow reversal of streamlines for a single sphere and of the relative trajectory for a pair; this phenomenon has been examined for pair interactions by Zurita-Gotor,

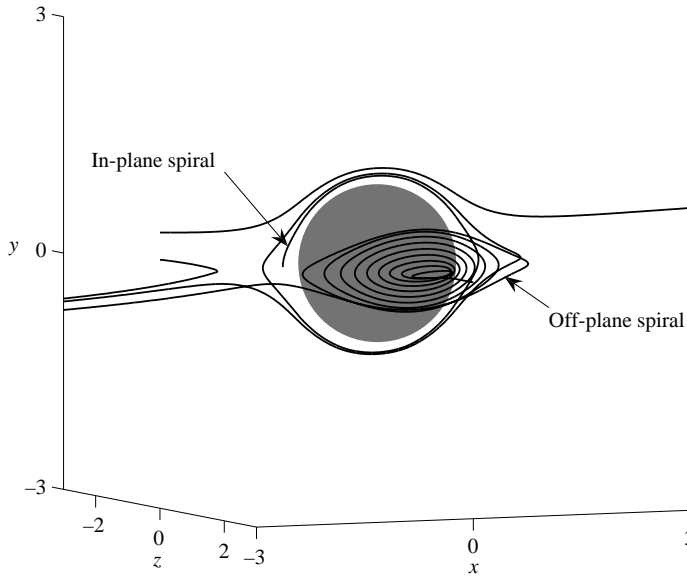


FIGURE 5. Three-dimensional streamline configuration around a freely rotating sphere in simple-shear flow at $Re = 0.5$ obtained by the LBM. Single open and reversing streamlines are shown, with one in-plane and one out-of-plane spiralling streamline also illustrated.

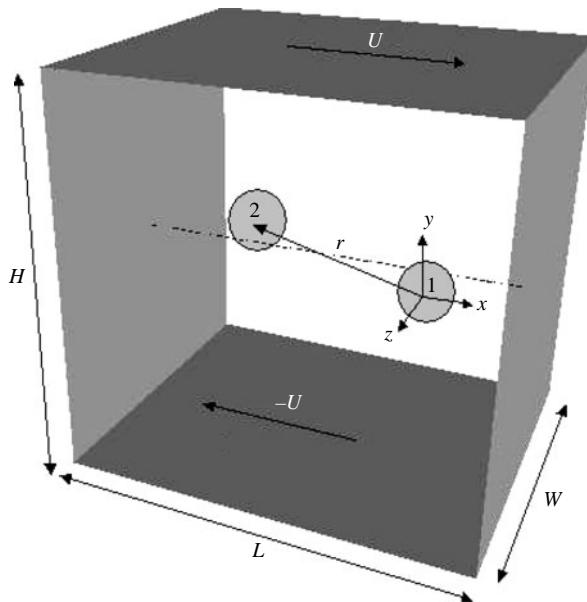


FIGURE 6. Sketch defining terms used in describing the pair-sphere motion in simple shear.

Bławdziewicz & Wajnryb (2007). Results will be presented below which address the influence of domain size in our work.

We have chosen a mesh density of 6.2 lattice nodes per radius of the sphere, and a computational domain of $20a \times 20a \times 20a$. Results have been found qualitatively independent of increase in the density of the lattice. To sample the trajectory space, we vary the initial positions of the spheres, with the pair symmetrically placed (except

in cases of unequal spheres) about the central point in the computational domain. We will usually describe the pair trajectories in terms of the time variation of the separation of the centres of the pair of spheres, $\mathbf{r}(t) = \mathbf{x}_2(t) - \mathbf{x}_1(t)$, with initial separation denoted by $\mathbf{r}_0 = (r_{0x}, r_{0y}, r_{0z})$.

Fluid inertia alters the topology of the trajectories of neutrally buoyant particles relative to the Stokes flow results outlined in §2.2. The trajectory space transitions from having two regions (open and closed) at $Re = 0$ to three types at any finite Re . These three trajectory types mirror the form of the streamlines of the steady finite- Re flow around a sphere and will again be termed open, reversing and spiralling. The motion is, of course, unsteady. We outline here the general results to be detailed in the following.

The *open trajectories* at finite Re are largely similar to those predicted for Stokes flow, starting from upstream infinity and progressing in the x (streamwise) direction in the same sense at every point, with some deflection of the trajectory when the pair is close. The open trajectories form the majority of the pair space, because the other types require significant particle interaction. Note that this does not imply closely approaching pairs will not have open trajectories: as seen below, spheres of equal size may approach surface separations below 1 per cent of a radius on open trajectories.

The *reversing trajectories* are much like the reversing (termed recirculating by Subramanian & Koch 2006*a, b*) streamlines about a single sphere discussed in detail by Mikulencak & Morris (2004). A pair with an initial offset ($r_{0x} < 0, r_{0y} > 0$) will approach and then reverse their relative positions in y and hence reverse their relative motion in x to recede toward ($r_x < 0, r_y < 0$).

The *spiralling trajectories* are divided into the in-plane and out-of-plane trajectories, depending upon whether the pair lie at the same or different z coordinates, respectively. For particles starting with a finite r_{0z} and lying near the vorticity axis (z), the pair approach one another along a path which spirals outward when projected onto the x - y plane, eventually leaving the mutual ‘zone of influence’ and moving away in x . For a pair lying at the same z , i.e. in the plane of shear, there is no z -directed motion because of the symmetry. There is a small region of pair space adjacent to contact in which the particles simply spiral around and away from one another, and then depart the close interaction. We note that the spiralling trajectory motion toward the shear plane is much like that of the fluid flow around a single sphere, where it is a requirement of mass conservation as material is being spun outward on and near the plane of shear and must be replaced by an inflow down the vorticity axis. The spiralling pair relative motion can thus be seen as an inertial hydrodynamic interaction driven by the centrifugal ejection of fluid in the equatorial plane region of the reference sphere.

Before we address the computational results, we present an argument which allows a fairly ready rationalization of the vanishing of closed trajectories for any $Re > 0$. This behaviour may be seen as a direct consequence of the loss of fore–aft symmetry, known from single-sphere shear-flow studies at finite inertia (Lin *et al.* 1970*b*; Mikulencak & Morris 2004; Subramanian 2006*a, b*), where the asymmetry is reflected in two diametrically opposed wakes in the downstream quadrants. As a result, streamlines, which would form a closed circuit around a freely rotating sphere at $Re = 0$ and thus must cross the $y = 0$ plane at the same distance from the sphere (at say \tilde{x} and $-\tilde{x}$), will at small Re suffer a slight streamwise displacement at each passing by the sphere. Because of the antisymmetry of the velocity on reflection through the origin, namely $\mathbf{u}(\mathbf{x}) = -\mathbf{u}(-\mathbf{x})$, a similar behaviour will occur at the next passage of the fluid element around the rotating sphere – the result of this is an outward

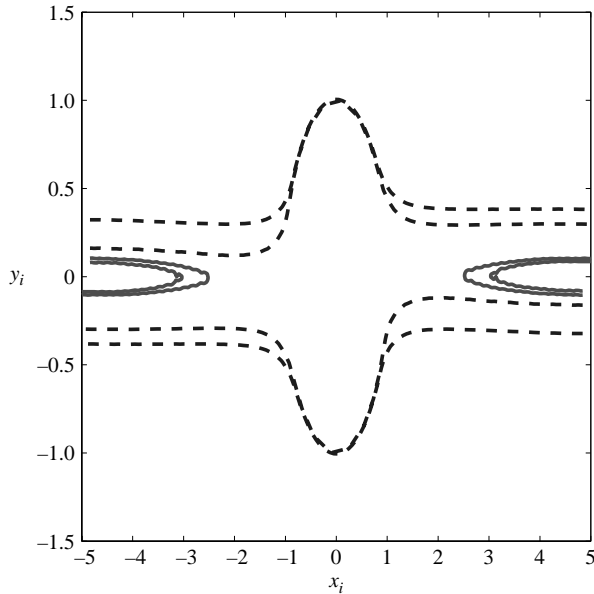


FIGURE 7. In-plane trajectories of a pair of equal-sized spheres of radius 1 in simple-shear flow at $Re = 0.1$ starting at the same streamwise but different gradient separations. Open trajectories are denoted by dashed lines and reversing by solid lines. Note that, in this figure the frame of reference is fixed at the centre of computation box to give the idea of motion of the two particles.

spiral. Similarly, at small Re a pair will have a fore–aft asymmetric interaction; even if the trajectories make circuits, these will cross the $y = 0$ plane at progressively larger values until the pair spiral away to infinite separation.

4.1. Finite Re trajectories in the shear plane

We begin by considering particles of equal size confined to the shear plane, $z = 0$. If the two particles start with large initial separation in x and y , only open and reversing trajectories will be observed. Figure 7 illustrates the nature of in-plane trajectories at $Re = 0.1$, beginning with small r_{0y} and $r_{0x} = -9.7$, i.e. a separation of almost ten radii in the streamwise direction. In this case, we illustrate both particle trajectories, with x_i and y_i denoting the coordinates of particle i ($i = 1$ or 2). The observed bumpiness in the trajectories is related to the mesh density of the sphere and resulting perturbations in the flow field due to the uncovering of the solid nodes as the particles move.

For a given Re , there is a critical gradient displacement, r_{0y}^c , that separates the two types of configurations. In the case of an open trajectory, the particles show evidence of fluid inertia, as there is a local deflection toward the zero-velocity ($y = 0$) plane upon close approach, and a net positive displacement in the gradient direction ($\Delta y > 0$) through the complete interaction which depends on r_{0y} : for smaller $r_{0y} > r_{0y}^c$, the particles come closer and experience a greater net displacement Δy . It is of interest to note that Kromkamp *et al.* (2005), in two-dimensional simulations, found a net displacement of the opposite sign, i.e. $\Delta y < 0$, for pairs interacting on open trajectories for $St > Re > 0$; Subramanian & Brady (2006) considered $Re = 0$ and finite St and

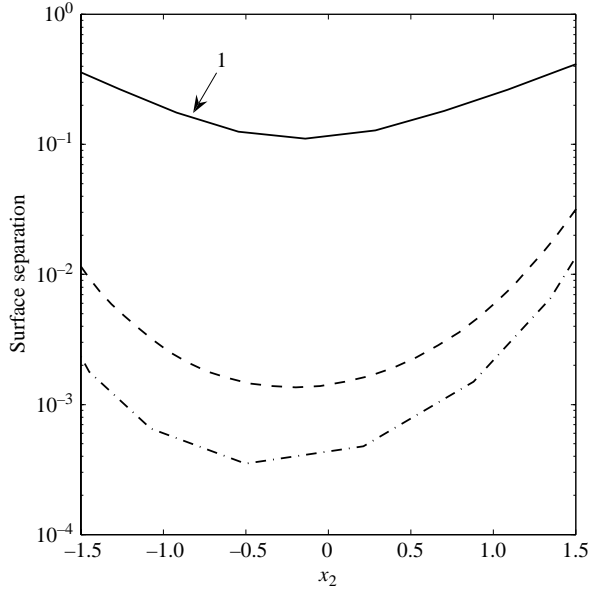


FIGURE 8. Surface separation ($(|\mathbf{r}| - 2a)/a$) between the spheres for different open trajectories at $Re = 0.1$. The trajectory labelled 1 does not involve modelled lubrication (surface separation $> 2/3$ lattice spacing) while the others do.

found a negative gradient displacement scaling as $St^{1/2}$ for small St . These results both lead to the conclusion that approaching particles at elevated inertia relative to the surrounding material, i.e. $St > Re$, reach smaller separations when resisted only by viscous stresses, and considering the results of the Stokes pair trajectory of figure 1(b), it is natural that they exit the interaction at a smaller y displacement than they had upstream of the interaction.

A closer examination of the trajectory asymmetry is made by considering the separation between sphere surfaces $(|\mathbf{r}| - 2a)/a$. These are plotted against the x coordinate of particle 2 in a frame fixed on particle 1 in figure 8 for three open trajectories. The closeness of approach leads to concern that the key feature of the gradient offset may be due to inaccurate computation of the lubrication force. However, for trajectory 1 the surface separation between the particles remains greater than 0.7 lattice units, so that modelled lubrication forces do not become active in the simulation of the motion. This trajectory is the least asymmetric of the three but shows a gradient offset nonetheless, and the lack of lubrication indicates that fluid inertia is responsible for the asymmetry.

Upon increasing the Reynolds number, keeping all other parameters fixed, r_{0y}^c increases: there is a larger region of reversing pair trajectories as Re increases, and this is consistent with the region of reversal approaching the particle more closely with increasing Re (Mikulencak & Morris 2004). To illustrate the implications of increasing Re for this region of trajectory bifurcation, trajectories for $Re = 0.1$ and 0.2 initiated at the same three positions are shown in figure 9 for three cases. Hereafter, results are presented in the relative form, $\mathbf{r} = \mathbf{x}_2 - \mathbf{x}_1$; the figure shows the reference particle 1 as a shaded elliptical region because of the stretching of the y coordinate. When particle 2 starts at A, $\mathbf{r}_0 = (-9.7, 0.65, 0)$, the higher Re trajectory brings it closer to the x -axis before it passes over the reference particle. For the particle

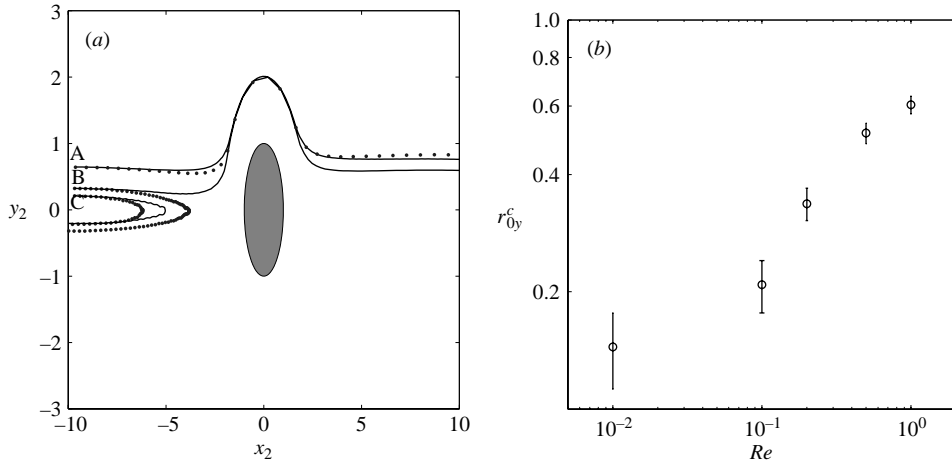


FIGURE 9. (a) In-plane trajectories of a pair of equal-sized spheres of unit radius in simple-shear flow at $Re = 0.1$ (solid lines) and $Re = 0.2$ (dotted lines). A trajectory for each of the two Re commences from A, $\mathbf{r}_0 = (-9.7, 0.65, 0)$; B, $\mathbf{r}_0 = (-9.7, 0.3, 0)$; and C, $\mathbf{r}_0 = (-9.7, 0.2, 0)$. (b) Log-log plot of the trajectory-bifurcation point r_{0y}^c separating open and reversing trajectories with Re for $x = -9.7$.

starting at B, $\mathbf{r}_0 = (-9.7, 0.3, 0)$, this tendency to move toward the x -axis is carried to the point of a flow reversal: at $Re = 0.1$ this initial condition lies on an open trajectory, while at $Re = 0.2$ it lies on a reversing trajectory. The particle starting at C, $\mathbf{r}_0 = (-9.7, 0.2, 0)$, with $Re = 0.1$ travels a greater horizontal distance before it reverses its direction than does the $Re = 0.2$ particle. It should be noted that the stagnation point associated with closest approach of a pair exhibiting trajectory reversal is found closer to contact with increasing Re (Poe & Acrivos 1975; Mikulencak & Morris 2004). The trajectories emanating from point C do not contradict this point, but there is potential for confusion. The reader should note that the width in y of the reversal zone at a given r_x increases with Re and this brings trajectories closer to contact as Re increases; comparing the B trajectory at $Re = 0.2$ with the C trajectory at $Re = 0.1$ helps in seeing this point. This is further illustrated in figure 9(b), where we plot the trajectory-bifurcation point r_{0y}^c with Re for $x = -9.7$. The error bar indicates the numerical precision in the measurement of r_{0y}^c . The value of r_{0y}^c increases roughly as $Re^{0.3}$ for $0.01 < Re < 1$, but for $Re \leq 0.01$ wall effects start to affect the nature of trajectories and for $Re > 0.5$, trajectories are increasingly influenced by the periodic images of the particles.

As noted, the boundaries may play a role in generating reversing trajectories even in Stokes flow as shown in Zurita-Gotor *et al.* (2007), and may also alter the rotation rate of a single particle at finite Re (Ding & Aidun 2000; Zettner & Yoda 2001; Mikulencak & Morris 2004). To assess the influence of the walls, we performed simulations with $H = 30$ (non-dimensionalized by radius of the sphere a) rather than 20 at $Re = 0.1$, keeping other parameters constant and found that the trajectories were indistinguishable. With an increase in size of the computation box in the flow direction to $L = 30$, r_{0y}^c increases, but the qualitative picture remains the same. With an increase in the domain size in the vorticity direction to $W = 30$, the trajectories are found to be unchanged.

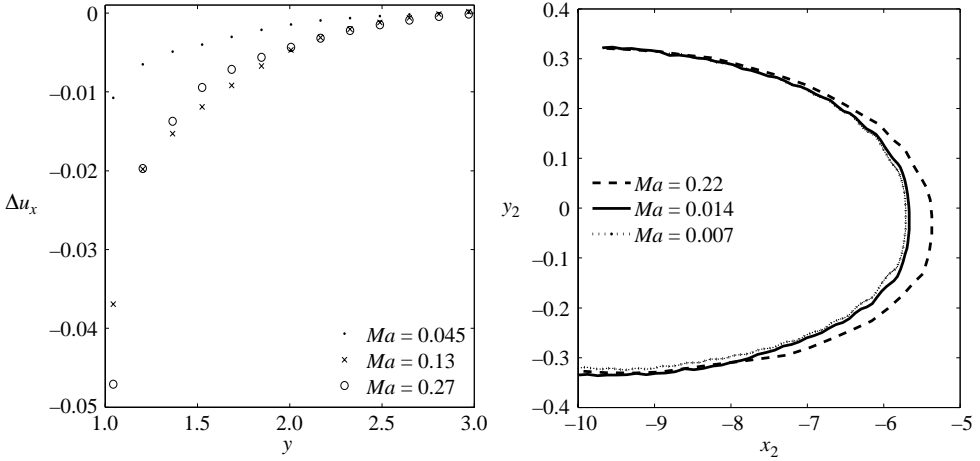


FIGURE 10. (a) The difference velocity in the flow direction $\Delta u_x(x=0, y, z=0)$ at $Ma=0.0225$ and at $Ma=0.045, 0.13$ and 0.27 plotted with the y coordinate for a single particle in simple-shear flow at $Re=0.1$. (b) The reversing pair trajectories at $Re=0.5$ for $Ma=0.007, 0.014$ and 0.22 .

Compressibility is inherent in the LBM as employed here and its influence upon our results was checked by simulation of a single particle and a pair of particles in simple-shear flow at various Mach numbers, $0.007 \leq Ma < 0.3$. As a technical matter, note that to vary Ma while keeping Re and a/H fixed, it is necessary to change the viscosity of the simulated fluid. The case of a single particle at $Re=0.1$ is considered in figure 10(a). The difference velocity in the flow direction is defined $\Delta u_x = u_x(Ma=0.0225) - u_x(Ma)$ and values of $Ma=0.045, 0.135$, and 0.27 are considered; the difference velocity along a line passing through the centre of the particle, $\Delta u_x(x=0, y, z=0)$ is plotted (for $y > 0$ only due to symmetry of the flow). It is seen that Δu_x grows considerably with Ma in the vicinity of the particle, but tends rapidly to zero away from the surface. In the case of a pair of particles, reversing pair trajectories are considered suitable for the comparison at different Ma , for the reason that they do not involve modelled near-field lubrication forces to complicate the analysis further. Figure 10(b) shows the reversing trajectories for $Ma=0.007, 0.014$ and 0.22 at $Re=0.5$. The pair at higher Ma approaches more closely in the flow direction before reversing its path. To suppress such effects, we keep $Ma < 0.1$ in our simulations, but it is important to bear in mind that small but non-negligible effects of compressibility remain down to $Ma = O(0.01)$.

We consider now the spiralling trajectories. If the two particles begin with a very small separation in the shear plane, the expectation is that they spiral around each other before departing the close interaction. However, it is unclear that for equal- or nearly equal-radius spheres the in-plane spiralling motion is present at $Re=0.1$. The spiralling trajectories in the plane of shear, if present, are compressed to an extremely small volume of trajectories which begin from pairs essentially in contact. When the Reynolds number is decreased, the reversal zone does not approach the contact surface so closely, and the expected spiralling trajectories are more readily observed. For $Re=0.01$, figure 11(a) shows a spiralling trajectory originating from $\mathbf{r}_0 = (-2.16, 0, 0)$, a surface separation of 0.16 radii, as it makes a partial circuit and then departs to infinity. The minimum surface separation between the spheres for this case is seen in figure 11(b) to be 3×10^{-5} . For minimum surface separations of

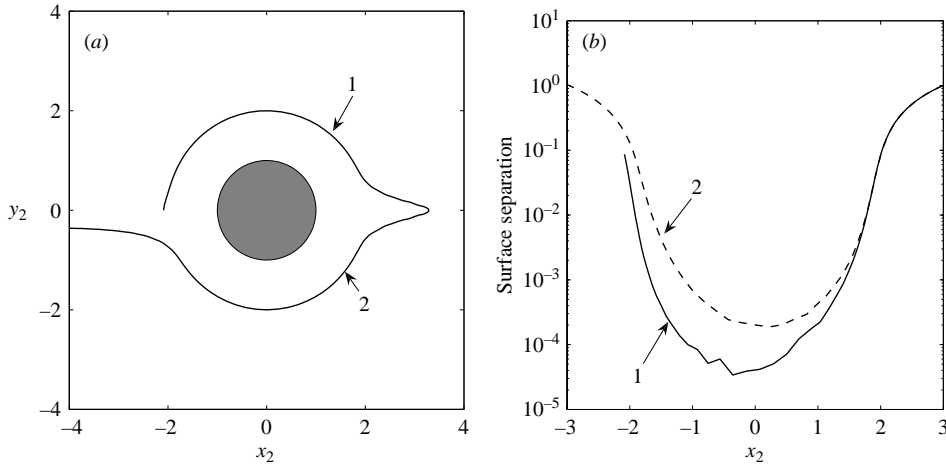


FIGURE 11. (a) The in-plane spiralling trajectory of equal-radius spheres originating from $r_0 = (-2.16, 0, 0)$ for $Re = 0.01$ in simple-shear flow. (b) Surface separation from this trajectory. The labels 1 and 2 denote segments progressing in the same sense with respect to the x direction.

$O(10^{-4})$, the spheres are observed always to separate at this Re . We note that in Stokes flow, the minimum separation of in-plane closed trajectories is about 5×10^{-5} radii (da Cunha & Hinch 1996). It is also of interest to note that in the experimental study of Darabaner & Mason (1967), in which the relative trajectories of two spheres in a circular shear flow under much weaker inertia of $Re = O(10^{-6})$ were studied, the need for this very close initial condition for ‘closed’ trajectories was observed. In that study, if an electric field was used to bring the two spheres to apparent contact, in subsequent shearing the spheres were found to make permanent orbiting doublets of a form similar to that predicted by the analysis of Batchelor & Green (1972). Without the application of an electric field, the spheres did not reach the necessary minimum separation and hence separated immediately upon shearing.

Figure 12(a) shows a spiralling trajectory for a pair with radius ratio of 2.3 at $Re = 0.01$. The corresponding surface separations for various portions of the curve are labelled. These indicate the portions of the trajectory over which the relative velocity has the same sign in the x coordinate. As the pair makes a full circuit, the pair separation increases and this is seen in more detail in figure 12(b).

4.2. Off-plane trajectories

We term the trajectories not residing in the shear plane ‘off-plane.’ At $Re = 0$, the xy -projections of the off-plane trajectories have a similar appearance to those in the shear plane, i.e. the presence of closed and open trajectories with a limiting closed trajectory separating the two. Over a complete circuit, these have zero displacement, $\Delta z = 0$. Any finite Re , however, breaks this symmetry and the trajectories are no longer closed. Again, there are three types of trajectories, namely reversing, open and spiralling. In the following discussion, the behaviour of trajectories is described for $r_{0z} > 0$ and the arguments can be extended for $r_{0z} < 0$ from the symmetry across the shear plane.

4.2.1. Reversing trajectories

For a fixed r_{0x} ($r_{0x} = -9.7$ was the usual case), various initial vorticity coordinates r_{0z} were studied. For $r_{0z} = 0$, the net vorticity displacement $\Delta z = 0$ as symmetry requires

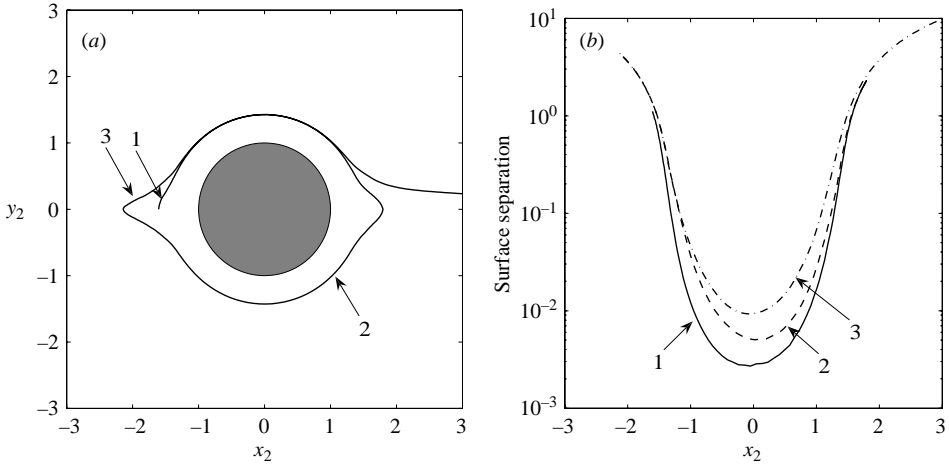


FIGURE 12. (a) The in-plane spiralling trajectory originating from $(-1.6, 0, 0)$ at $Re = 0.01$ for a pair of spheres with radius ratio of 2.3 in simple shear flow. (b) Surface separation from this trajectory. The labels 1, 2, and 3 denote segments progressing in the same sense with respect to the x direction.

no motion in z . For small finite r_{0z} , the net vorticity displacement (Δz) of the reversing trajectories is negative while at higher r_{0z} , Δz changes sign and becomes positive. We present this observation without having sought to delineate the initial separation surface leading to $\Delta z < 0$ because of the domain dependence and the dependence on the manner of releasing the particle (the initial condition).

4.2.2. Open trajectories

Following the arguments given for in-plane trajectories, if the initial displacement in the flow direction is fixed, one expects a critical displacement $r_{0y}^c(z)$ for every z -plane which sets the reversing trajectories apart from the open ones; this initial separation point lies on the separatrix between open and reversing trajectories. We begin by looking at the vorticity displacement (Δz) of the off-plane open trajectories. All open trajectories with $r_{0z} > 0$ are found to have a net positive Δz , meaning they are displaced away from the shear plane through the pair interaction.

The xy -projection of the off-plane open trajectories is now considered. For small values of r_{0z} , the open trajectories are visually very similar to the open trajectories in the shearing plane for the same value of gradient displacement r_{0y} . As the initial separation is taken with larger r_{0z} , the pair trajectory exhibits a decreasing gradient displacement Δy , as illustrated by figure 13 for the open trajectories starting at $r_{0z} = 0, 0.032$ and 1.9 .

4.2.3. Spiralling trajectories

The most visually prominent effect of inertia upon the pair-trajectory space is the introduction of spiralling trajectories along the vorticity axis. The term spiralling refers to a trajectory which increases in distance from the z -axis as the pair z separation decreases. An xy -projection of such a trajectory cuts the x -axis successively, for example, at x_1 and x_2 with $|x_2| > |x_1|$, and a similar statement may be made for the crossing of the y -axis in this projection. A pair originating from a point at separation in z of a few radii, and only slightly displaced from the z -axis, will spiral towards the shear plane. Following their closest approach, the pair move away with the shear

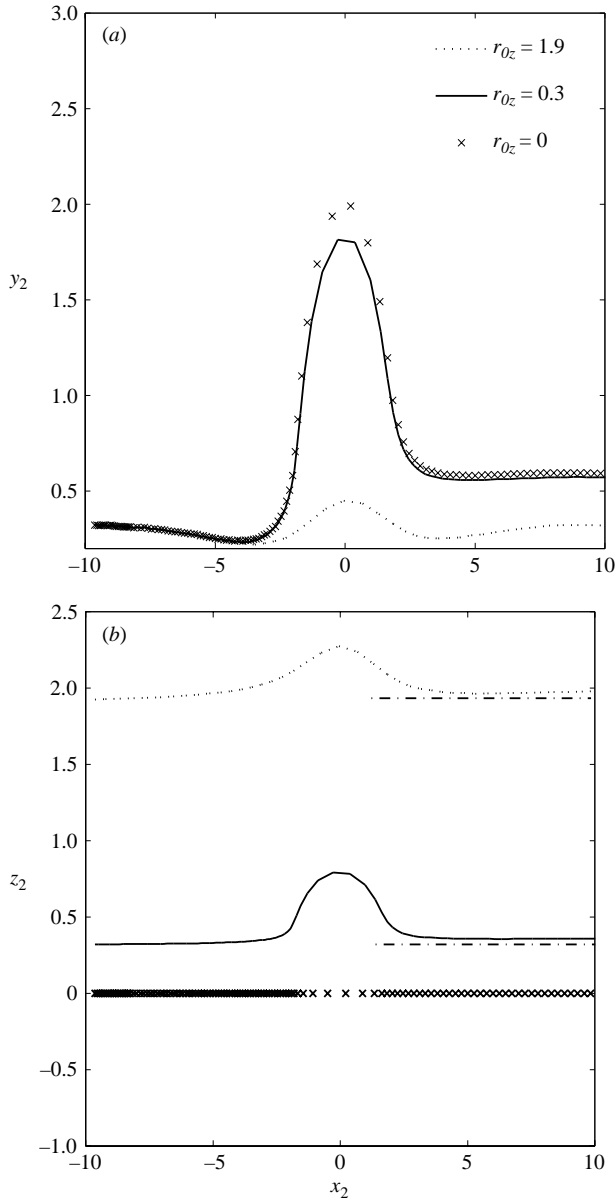


FIGURE 13. Open trajectories starting from $(-9.7, 0.3, r_{0z})$ for $r_{0z} = 0, 0.3$ and 1.9 at $Re = 0.1$ (a) xy -projection (b) xz -projection. For reference, the dashed-dotted line is at the original vorticity separation, and the deviation of the curves from this line illustrates the vorticity displacement Δz . For the trajectory with $r_{0z} = 0$, the points are equally spaced in time, and hence look denser upon approach than separation because of the positive gradient displacement.

flow to infinite separation. Early in this trajectory, the motion has two components, along the z -axis towards the plane of shear and spiralling in the local x - y plane. Suppose the initial displacement is $\mathbf{r}_0 = (0, r_{0y}, r_{0z})$. For a trajectory with smaller r_{0y} , the z -directed motion is more pronounced than the spiralling and thus there is a limiting trajectory that coincides with the z -axis and does not spiral. This motion

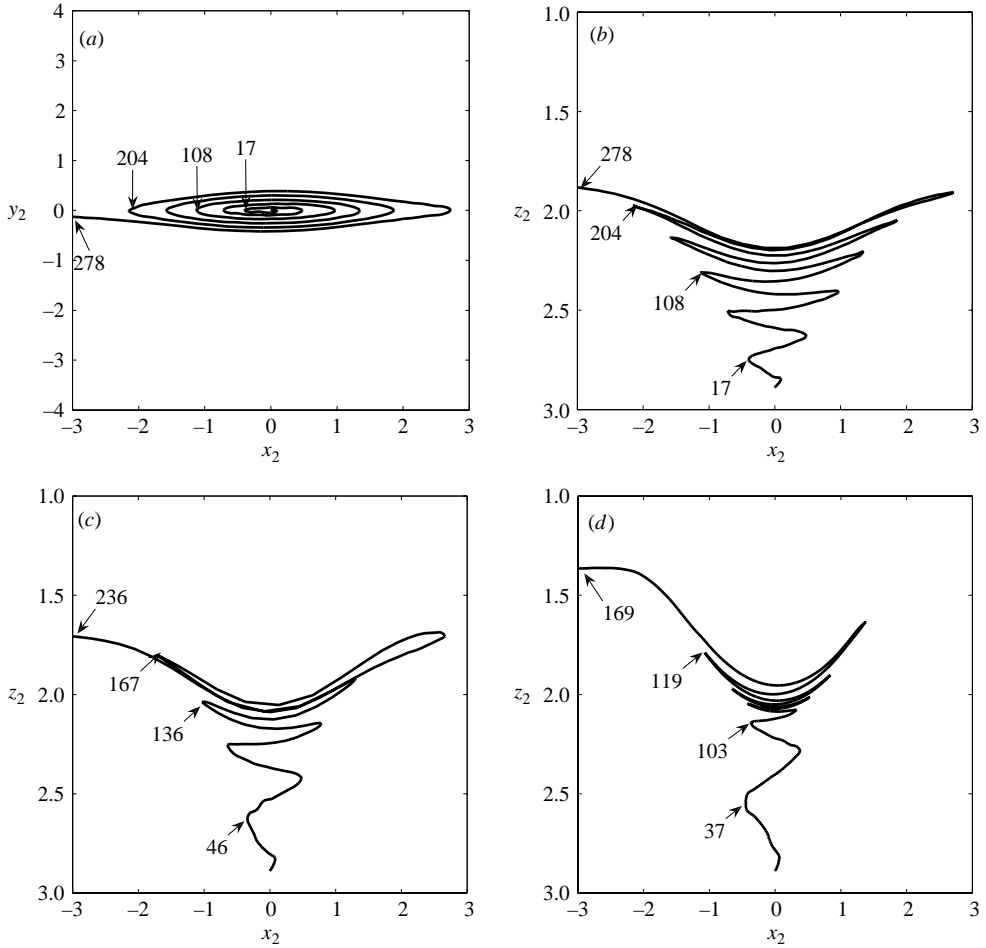


FIGURE 14. Off-plane spiralling trajectories starting from $\mathbf{r}_0 = (-0.0032, 0.016, 2.9)$ for (a) $Re = 0.1$, xy -projection, (b) $Re = 0.1$, xz -projection, (c) $Re = 0.2$, xz -projection, (d) $Re = 0.5$, xz -projection. The arrows indicate the strain ($\dot{\gamma}t$) values where the trajectory crosses $y = 0$ for $x < 0$ as illustrated in (a). Strain (or t) is zero at \mathbf{r}_0 .

presumably would be unstable to any displacement outward (in x or y), which would yield a spiral motion.

Figure 14 shows trajectories with $\mathbf{r}_0 = (-0.0032, 0.016, 2.9)$. First consider figure 14(a, b) for $Re = 0.1$ in xy - and xz -projections, respectively. The two particles spiral toward one another along the vorticity axis. Following a close encounter, the particles move off toward infinite separation in opposite directions of the shear flow. Examination of the xz -projection of the trajectory shows that initially it has only negative z -velocity but as the pair becomes close, the z -directed relative motion changes sign during each circuit, while still bringing the pair closer over each full circuit. This motion is quite similar to that of a fluid element around a freely rotating sphere seen in §3. Hence the streamline configuration around a single sphere (shown in figure 5) should aid in understanding the pair behaviour at Re larger than computed here.

We now consider the xz -projections of spiralling trajectories at $Re = 0.1, 0.2$ and 0.5 , shown respectively in figure 14(b–c). The strain undergone by the flow ($\dot{\gamma}t$) at

points along the trajectories is labelled with $t=0$ at the initial separation, \mathbf{r}_0 . Note that the initial separation is the same for each of these conditions. For the trajectory at largest $Re=0.5$, the advance along the z -axis is more rapid, and the particles approach one another and complete the close interaction at the smallest value of the strain. The observation of a larger strain to complete the close interaction at smaller Re is consistent with the $Re=0$ prediction that the interaction would be a closed trajectory, and would take place at a bounded separation for infinite strain.

Before closing this section, we note that the finite Re pair trajectories are functions of initial conditions (history-dependent). Our approach has been to allow the spheres to reach a steady rotation rate, i.e. the hydrodynamic torque relaxes to zero, at fixed \mathbf{r}_0 prior to allowing translation. The equilibration time scales as $\tau_{eq} = H^2/\nu$, the time required for diffusion of momentum from the walls to the centre, where ν is the kinematic viscosity of the fluid. One could also set the body in motion with the velocity of the fluid which would be at its centre point under the assumption this reduces the hydrodynamic force, but this is a poor condition for very close pairs such as those seen in the in-plane spiralling case. It was judged prudent to use the single initial condition of torque relaxation in all cases. This is admittedly not a completely accurate representation of the free trajectories, but we have found that the far-field open and reversing trajectories obtained with and without torque equilibration are indistinguishable.

5. Conclusions

The hydrodynamic interactions of a pair of spherical particles suspended in simple-shear flow at finite Re is a basic issue important to development of the understanding of inertia in suspension mechanics. While it is not feasible to map the entire trajectory space numerically even for a single Re , by focusing on $Re = O(0.1)$, we have delineated the structure of the finite Re pair trajectory space for neutrally buoyant spheres of equal size. The similarity of the various forms of trajectory seen in the pair space to the streamlines around a single freely rotating sphere provides some guidance in considering the pair interaction at larger Re .

Using the LBM with a wall-bounded geometry with periodicity in the flow and vorticity direction, we have demonstrated the characteristics of finite inertial pair trajectories in simple shear flow. The role of the boundary is found to be minimal for wall separations of ten particle diameters at $Re = O(0.1)$, while the periodicity in the flow direction has some quantitative effects. The periodicity in the vorticity direction has a negligible effect upon the in-plane trajectories presented but may alter the quantitative results for off-plane trajectories.

For the range of Reynolds numbers $O(10^{-2}) < Re < O(1)$ studied, the simulated trajectories were qualitatively much different from those at $Re=0$. The closed pair trajectories (Batchelor & Green 1972) present at $Re=0$ vanish at finite inertia, a result which in hindsight can largely be deduced from the loss of the fore-aft symmetry of Stokes flow. The inertia gives rise to new classes of pair relative trajectories which are similar to the reversing (Mikulenck & Morris 2004) and spiralling (Subramanian & Koch 2006*a, b*) streamlines around a freely rotating sphere. The open trajectories occupy most of the pair-trajectory space and are fore-aft asymmetric at finite Re , giving always a positive offset in the gradient direction for neutrally buoyant particles. The reversing and spiralling trajectories, which replace the closed trajectories predicted at $Re=0$, occupy a smaller volume of pair-trajectory space. In fact, at $Re \geq 0.1$, the

in-plane spiralling trajectories have not been observed in our calculations, although it is not expected that they completely vanish.

This study of particle interactions due to inertial hydrodynamics may have relevance to examination of structures seen in bulk suspension flows. In earlier work, the flow around a single sphere at finite Re , and in particular the reversing streamlines, was invoked to suggest pair-trajectory reversal as a possible basis for the formation of trains of particles in pressure-driven flow in a pipe (Matas *et al.* 2004). The reversing pair trajectories presented here provide a better guide to consideration of this issue. In more general terms, our study serves as a step towards developing theoretical understanding of the role of inertia at the particle scale in particle-laden flows.

This work was supported by NSF Cooperative Agreement No. HRD-0206162, to the CREST Center for Mesoscopic Modeling and Simulation at CCNY. We are grateful to Professor A. J. C. Ladd of the University of Florida for providing the initial lattice-Boltzmann code.

REFERENCES

- AIDUN, C. K., LU, Y. & DING, E. 1998 Direct analysis of particulate suspensions with inertia using the discrete Boltzmann equation. *J. Fluid Mech.* **373**, 287–311.
- BACHELOR, G. K. 1977 The effect of Brownian motion on the bulk stress in a suspension of spherical particles. *J. Fluid Mech.* **83**, 97–117.
- BACHELOR, G. K. & GREEN, J. T. 1972 The hydrodynamic interaction of two small freely-moving spheres in a linear flow field. *J. Fluid. Mech.* **56**, 375–400.
- BRADY, J. F. & BOSSIS, G. 1988 Stokesian Dynamics. *Annu. Rev. Fluid Mech.* **20**, 111–157.
- BRADY, J. F. & MORRIS, J. F. 1997 Microstructure of strongly sheared suspensions and its impact on rheology and diffusion. *J. Fluid. Mech.* **348**, 103–139.
- BRENNER, H. & O'NEILL, M. E. 1972 On the Stokes resistance of multiparticle systems in a linear shear field. *Chem. Engng Sci.* **27**, 1421.
- CHUN, B. & LADD, A. J. C. 2006 Inertial migration of neutrally buoyant particles in a square duct: An investigation of multiple equilibrium positions. *Phys. Fluids* **18**, 031704.
- DA CUNHA, F. R. & HINCH, E. J. 1996 Shear-induced dispersion in a dilute suspension of rough spheres. *J. Fluid Mech.* **309**, 211–223.
- DARABANER, C. L. & MASON, S. G. 1967 Particle motions in sheared suspensions XXII: Interaction of rigid spheres (Experimental). *Rheol. Acta.* **6**, 273–284.
- DING, E. & AIDUN, C. K. 2000 The dynamics and scaling law for particles suspended in shear flow with inertia. *J. Fluid Mech.* **423**, 317–344.
- FENG, J., HU, H. H. & JOSEPH, D. D. 1994 Direct simulation of initial value problems for the motion of solid bodies in a Newtonian fluid. Part 2. Couette and Poiseuille flows. *J. Fluid Mech.* **277**, 271–301.
- FRISCH, U., D'HUMIÈRES, D., HASSLACHER, B., LALLEMAND, P., POMEAU, Y. & RIVET, J. P. 1987 Lattice gas hydrodynamics in two and three dimension. *Complex Systems* **1**, 649.
- HIGUERA, F., SUCCI, S. & BENZI, R. 1989 Lattice gas dynamics with enhanced collisions. *Europhys. Lett.* **9**, 345–349.
- HU, H. H. 1996 Direct simulation of flows of solid-liquid mixtures. *Intl J. Multiphase Flow* **22**, 335–352.
- HU, H. H., JOSEPH, D. D. & CROCHET, M. J. 1992 Direct simulation of fluid particle motions. *Theor. Comput. Fluid Dyn.* **3**, 285–306.
- HU, H. H., PATANKAR, N. A. & ZHU, M. Y. 2001 Direct numerical simulations of fluid-solid systems using the arbitrary Lagrangian-Eulerian technique. *J. Comput. Phys* **169**, 427–462.
- HUANG, P. Y. & JOSEPH, D. D. 2000 Effects of shear thinning on migration of neutrally-buoyant particles in pressure driven flow of Newtonian and viscoelastic fluid. *J. Non-Newtonian Fluid Mech.* **90**, 159–185.
- JEFFREY, D. J. 1992 The calculation of the low Reynolds number resistance functions for two unequal spheres. *Phys. Fluids A* **4**, 16–29.

- JEFFREY, D. J. & ONISHI, Y. 1984 Calculation of the resistance and mobility functions for two unequal rigid spheres in low-Reynolds-number flow. *J. Fluid Mech.* **139**, 261–290.
- KIM, S. & MIFFLIN, R. T. 1985 The resistance and mobility functions of two equal spheres in low-Reynolds-number flow. *Phys. Fluids* **28**, 2033–2045.
- KOCH, D. L. & HILL, R. J. 2001 Inertial effects in suspension and porous media flows. *Annu. Rev. Fluid Mech.* **33**, 619–647.
- KOSSACK, C. & ACRIVOS, A. 1974 Steady simple shear flow past a circular cylinder at moderate Reynolds number: a numerical solution. *J. Fluid Mech.* **66**, 353–376.
- KROMKAMP, J., VAN DEN ENDE, D. T. M., KANDHAI, D., VAN DER SMAN, R. G. M. & BOOM, R. M. 2005 Shear-induced self-diffusion and microstructure in non-Brownian suspensions at non-zero Reynolds number. *J. Fluid Mech.* **529**, 253–278.
- LADD, A. J. C. 1988 Hydrodynamic interactions in a suspension of spherical particles. *J. Chem. Phys.* **88**, 5051–5063.
- LADD, A. J. C. 1994a Numerical simulations of particulate suspensions via a discretized Boltzmann equation. Part 1. Theoretical foundation. *J. Fluid Mech.* **271**, 285–309.
- LADD, A. J. C. 1994b Numerical simulations of particulate suspensions via a discretized Boltzmann equation. Part 2. Numerical results. *J. Fluid Mech.* **271**, 311–339.
- LADD, A. J. C. & VERBERG, R. 2001 Lattice-Boltzmann simulations of particle-fluid suspensions. *J. Statist. Phys.* **104**, 1191–1151.
- LEAL, L. G. 1992 *Laminar Flow and Convective Transport Processes*. Butterworth-Heinemann.
- LIN, C. J., LEE, K. J. & SATHER, N. F. 1970a Slow motion of two spheres in a shear field. *J. Fluid Mech.* **43**, 35–47.
- LIN, C. J., PEERY, J. H. & SCHOWALTER, W. R. 1970b Simple shear flow round a rigid sphere: Inertial effects and suspension rheology. *J. Fluid Mech.* **44**, 1–17.
- MATAS, J., GLEZER, V., GUAZZELLI, E. & MORRIS, J. F. 2004 Trains of particles in finite-Reynolds-number pipe flow. *Phys. Fluids* **16**, 4192–4195.
- MIKULENCAK, D. R. & MORRIS, J. F. 2004 Stationary shear flow around fixed and free bodies at finite Reynolds number. *J. Fluid Mech.* **520**, 215–242.
- NGUYEN, N. Q. & LADD, A. J. C. 2002 Lubrication corrections for lattice-Boltzmann simulation of particle suspensions. *Phys. Rev. E* **66**, 046708.
- NIRSCHL, H., DWYER, H. A. & DENK, V. 1995 Three-dimensional calculations of the simple shear flow around a single particle between two moving walls. *J. Fluid Mech.* **283**, 273–285.
- POE, G. G. & ACRIVOS, A. 1975 Closed streamline flows past rotating single spheres and cylinders: inertia effects. *J. Fluid Mech.* **72**, 605–623.
- ROBERTSON, C. R. & ACRIVOS, A. 1970 Low Reynolds number shear flow past a rotating circular cylinder. Part 1. Momentum transfer. *J. Fluid Mech.* **40**, 685–703.
- SUBRAMANIAN, G. & BRADY, J. F. 2006 Trajectory analysis for non-Brownian inertial suspensions in simple shear flow. *J. Fluid Mech.* **559**, 151–203.
- SUBRAMANIAN, G. & KOCH, D. L. 2006a Centrifugal forces alter streamline topology and greatly enhance the rate of heat and mass transfer from neutrally buoyant particles to a shear flow. *Phys. Rev. Lett* **96**, 134503.
- SUBRAMANIAN, G. & KOCH, D. L. 2006b Inertial effects on the transfer of heat or mass from neutrally buoyant spheres in a steady linear velocity field. *Phys. Fluids* **18**, 073302.
- SWAMINATHAN, T. N., MUKUNDAKRISHNAN, K. & HU, H. H. 2006 Sedimentation of an ellipsoid inside an infinitely long tube at low and intermediate Reynolds numbers. *J. Fluid Mech.* **551**, 357–385.
- WAKIYA, S., DARABANER, C. L. & MASON, S. G. 1967 Particle motions in sheared suspensions XXI: Interaction of rigid spheres (Theoretical). *Rheol. Acta.* **6**, 273–284.
- ZARRAGA, I. E. & LEIGHTON, D. T. 2001 Normal stress and diffusion in a dilute suspension of hard spheres undergoing simple shear. *Phys. Fluids* **13**, 565–577.
- ZETTNER, C. M. & YODA, M. 2001 The circular cylinder in simple shear at moderate Reynolds number: An experimental study. *Exps. Fluids* **30**, 346–353.
- ZURITA-GOTOR, M., BŁAWZDZIEWICZ, J. & WAJNRYB, E. 2007 Swapping trajectories: a new cross-streamline particle migration mechanism in a dilute suspension of spheres. *J. Fluid Mech.* **592**, 447–469.